



Predicting CO₂–water interfacial tension under pressure and temperature conditions of geologic CO₂ storage

Laura C. Nielsen ^{*}, Ian C. Bourg, Garrison Sposito

Geochemistry Department, Lawrence Berkeley National Laboratory, Earth Sciences Division, MS 90-1116, Berkeley, CA 94720, USA

Received 21 March 2011; accepted in revised form 12 December 2011; available online 19 December 2011

Abstract

Storage in subsurface geologic formations, principally saline aquifers, is currently under development as a major approach to counter anthropogenic CO₂ emissions. To ensure the stability and long-term viability of geologic carbon storage, injected CO₂ must be kept in place by an overlying cap rock of very low permeability. Capillary forces in the cap rock act to prevent upward migration and escape of the stored supercritical fluid, with interfacial tension (IFT) between the aqueous brine phase and the CO₂ phase being the primary control. However, published experimental CO₂–water IFT data vary widely, mainly because of inadequate experimental protocols or inappropriate use of bulk-fluid properties in computing IFT from experimental observations. Only two published data sets were found to meet all criteria of merit for an accurate measurement of IFT over the entire range of pressure (5–45 MPa) and temperature (298–383 K) pertinent to geologic carbon storage. In such circumstances, molecular simulations can enhance the utility of limited data when used to validate assumptions made in their interpretation, resolve discrepancies among data, and fill gaps where data are lacking. Simulations may also be used to provide insight into the relationship between IFT and fundamental properties, such as the strength of the CO₂–H₂O interaction. Through molecular dynamics simulations, we compared the quality of three CO₂ models and two H₂O models (SPC/E and TIP4P2005) in predicting IFT under the pressure and temperature conditions relevant to geologic CO₂ sequestration. Interfacial tension at fixed temperature simulated via molecular dynamics decreased strongly with increasing pressure below the critical CO₂ pressure of 7 MPa, then leveled off, in agreement with experiment, whereas increasing temperature from 300 to 383 K at fixed pressure had little effect on IFT, which is also consistent with experimental data. Our results demonstrated that the strength of the short-range portion of the CO₂–H₂O interaction exerts a major influence on IFT. The CO₂ model that best represented the attractive part of this interaction for randomly-oriented water molecules also best captures the experimental pressure dependence of IFT when combined with either water model. When combined with the SPC/E water model, this CO₂ model underestimated IFT by ~10 mN/m, which approximately equals the amount by which the SPC/E water model underestimates the surface tension of pure water. When combined with the TIP4P2005 water model, this model accurately captured the pressure dependence of the CO₂–H₂O IFT at 383 K over the entire pressure range examined. These pressure variations will have the dominant effect on IFT — especially at pressures lower than the CO₂ critical pressure (~7 MPa)—and, therefore, on the CO₂ storage capacity and sealing integrity of a subsurface reservoir.

© 2011 Elsevier Ltd. All rights reserved.

1. INTRODUCTION

Storage in subsurface geologic formations, such as deep saline aquifers or depleted hydrocarbon reservoirs, offers a

promising means of permanently sequestering anthropogenic CO₂ that can be readily incorporated into the current global energy infrastructure (IPCC, 2005). Subsurface storage of CO₂ currently emitted from point sources, such as coal-burning power plants, can potentially offset up to 12% of total emissions by 2020 and up to 45% by 2050 (IPCC, 2005). Proposed and existing CO₂ storage reservoirs are sealed against catastrophic loss to the atmosphere via

^{*} Corresponding author.

E-mail addresses: lnielsen@lbl.gov, lnielsen@berkeley.edu (L.C. Nielsen).

“structural trapping” involving a geologic formation of very low permeability (“cap rock”) that overlies the reservoir and prevents the upward volume flow of reservoir fluids (Bachu, 2000; Alkan et al., 2010). Cap rock sealing phenomena have major impacts on geologic CO₂ storage because they underlie the assessment of failure risk during the time required (centuries to millennia) for physical and chemical transformations of CO₂ in the reservoir to result in permanent sequestration.

Carbon dioxide injected into a reservoir is expected to rise buoyantly and accumulate beneath the cap rock. Its migration upward through the cap rock can occur via molecular diffusion, an inherently slow process (millennial time scales), or by volume (slow Darcy) flow, which would efficiently release stored CO₂ into the atmosphere once initiated (Li et al., 2005, 2006) and which therefore must be prevented. Volume flow occurs when the differential pressure across a cap rock exceeds its breakthrough pressure, above which CO₂ will overcome opposing capillary pressure, P_c (Pa), and push upward through natural pore throats within the cap rock (Li et al., 2005; André et al., 2007; Chiquet et al., 2007a; Leroy et al., 2010). Taking as an example CO₂ stored in a saline aquifer, we may express this capillary pressure by the standard Young–Laplace equation:

$$P_c = P_{\text{CO}_2} - P_{\text{brine}} = \frac{2\gamma\cos\phi}{R} \quad (1)$$

where γ (N/m) is the interfacial tension (IFT) on the boundary between the brine and CO₂ phases, ϕ (rad) is the wetting angle, and R (m) is a characteristic pore radius along a percolation pathway (Li et al., 2005, 2006; Chalbaud et al., 2009).

In hydrocarbon reservoirs, breakthrough pressures determined for natural reservoir gases may significantly overestimate that for carbon dioxide because the CO₂–brine IFT is smaller than any hydrocarbon–brine IFT (Li et al., 2005, 2006). Thus CO₂ must be injected and stored at lower pressures than natural gas to ensure the same sealing integrity, and evaluation of threshold injection pressure must be based on the relevant IFT. The experiments of Li et al. (2005) suggest that changes in breakthrough pressure caused by varying gas and brine composition are essentially proportional to changes in IFT. Beyond cap rock sealing capacity, the flow of carbon dioxide through reservoir rock and residual CO₂ trapping following plume imbibition also are strongly impacted by capillary effects. “Residual capillary trapping,” wherein CO₂ is immobilized as discrete bubbles in pores within reservoir rock, is considered a key mechanism for retaining reservoir CO₂ over the short-term, with none of the risk of catastrophic failure associated with structural trapping (Suekane et al., 2010; Pentland et al., 2011).

As shown by Eq. (1), interfacial tension and wetting angle both exert primary control on the capillary phenomena that determine the efficacy of structural and residual capillary trapping (Siemons et al., 2006; Chiquet et al., 2007b; Espinoza and Santamarina, 2010). The wettability of reservoir and cap rock materials plays a significant role in carbon dioxide flow and retention, and is a subject of

ongoing research (Siemons et al., 2006; Chiquet et al., 2007b; Espinoza and Santamarina, 2010). However, effective modeling of subsurface CO₂ flow and calculation of CO₂ storage capacity depends principally on knowledge of brine–CO₂ IFT over a range of pressures, temperatures, and brine compositions (Alkan et al., 2010). In this paper, we investigate the pressure and temperature dependence of water–CO₂ IFT and its molecular-scale origins. Our results are directly relevant to brine–CO₂ IFT because the salinity dependence of brine–CO₂ IFT is relatively small (~10% increase in IFT from 0 to 1.75 M NaCl; Chalbaud et al., 2009) and essentially identical to the well-known salinity dependence of brine–vapor surface tension (Chiquet et al., 2007a; Aggelopoulos et al., 2010).

1.1. The experimental IFT database

Common experimental techniques for measuring CO₂–brine and CO₂–water IFT include the pendant drop method (Andreas et al., 1938; Hauser and Michaels, 1948; Heuer, 1957; Wesch et al., 1997; da Rocha et al., 1999; Hebach et al., 2002; Tewes and Boury, 2004; Kvamme et al., 2007; Chiquet et al., 2007a; Bachu and Bennion, 2009; Chalbaud et al., 2009; Georgiadis et al., 2010), the capillary rise technique (Massoudi and King, 1974; Chun and Wilkinson, 1995), and the sessile drop method (Espinoza and Santamarina, 2010). In the pendant drop method, a small droplet of aqueous phase (water or brine) is extruded from a needle into CO₂ maintained at the desired P – T condition and the droplet shape is recorded. The drop shape profile is then analyzed to determine IFT (Andreas et al., 1938; Hauser and Michaels, 1948). To measure IFT via the capillary rise technique, a capillary tube is wetted by the aqueous phase and surface tension at the meniscus draws it up the capillary tube. After equilibration, IFT is calculated based on the height of capillary rise, capillary diameter, phase density difference (aqueous phase vs. CO₂), and wetting angle (e.g., Chun and Wilkinson, 1995). In the sessile drop method, a small drop of liquid is placed onto a solid surface immersed in CO₂ and droplet shape is recorded and analyzed to determine IFT (Espinoza and Santamarina, 2010). Calculation of IFT using any of these experimental methods requires that the density difference between CO₂ and the aqueous phase ($\Delta\rho$) be known.

Published experimental CO₂–water IFT values vary widely, especially those measured near the CO₂ critical point. Reviews of these data (Hebach et al., 2002; Kvamme et al., 2007; Chiquet et al., 2007a; Georgiadis et al., 2010) indicate that several factors significantly affect IFT determinations, and careful scrutiny of them in published studies is required in order to compile a critical database of experimental IFT data. In particular, aside from composition effects (e.g., impurities), IFT is sensitive to $\Delta\rho$, thermocouple position within the apparatus, and equilibration time.

1.2. Equilibrium CO₂ and H₂O densities

Chiquet et al. (2007a) observed that estimating CO₂ and water densities based on data for the pure phases yields major errors in IFT values at temperatures and pressures close

to those corresponding to the isopycnic point, at high pressures and low temperatures. Their graph comparing $\Delta\rho$ for CO₂ and water in contact vs. the pure phases shows clearly that large discrepancies (>10%) appear at pressures above ~20 MPa and temperatures below 343 K. Georgiadis et al. (2010) have recently argued in favor of using equations of state to estimate $\Delta\rho$, their view being that incorporating direct density measurements into the experimental determination of IFT by the pendant drop method introduces additional measuring uncertainties. Although the IFT data of Chiquet et al. (2007a) and Georgiadis et al. (2010) do agree well at 343 K (the only analysis temperature common to the two data sets) over a broad range of pressures, this temperature is just high enough to avoid large errors in estimating $\Delta\rho$ over the pressure range relevant to geologic CO₂ storage. In general, relying upon equations of state for pure phases can introduce significant variability in experimental IFT values. Therefore, IFT data above 20 MPa and below 345 K from studies wherein $\Delta\rho$ is based on equations of state for pure phases (e.g., Heuer, 1957; Massoudi and King, 1974; Chun and Wilkinson, 1995; Wesch et al., 1997; da Rocha et al., 1999; Hebach et al., 2002; Espinoza and Santamarina, 2010; Georgiadis et al., 2010) or on CO₂-saturated water and bulk CO₂ (Chalbaud et al., 2009) have been excluded from our critical database.

1.3. Temperature near the CO₂–H₂O interface

Hebach et al. (2002) found that the typical thermocouple positioning within the pendant drop apparatus on the autoclave wall introduces experimental artifacts, resulting in an abrupt drop, or cusp, in IFT near the CO₂ critical pressure. This cusp feature is not observed when the thermocouple is placed in close proximity to the CO₂–water interface (Hebach et al., 2002; Kvamme et al., 2007; Georgiadis et al., 2010), nor is it found in theoretical calculations (Li et al., 2008) or molecular simulations (Kvamme et al., 2007). Therefore, experimental reports having the cusp feature or that do not indicate the position of the thermocouple, and, of course, those that do not report the temperature near the CO₂–water interface (Heuer, 1957; Chun and Wilkinson, 1995; Wesch et al., 1997; da Rocha et al., 1999; Bachu and Bennion, 2009; Chalbaud et al., 2009) also have been excluded from our critical database.

1.4. Equilibration time

The value of IFT depends on the time of equilibration between the CO₂ and water phases. In the pendant drop and sessile drop methods, diffusion and chemical changes at the CO₂–water interface lead to drop-aging, altering interface morphology over time and causing a time-dependent IFT. This phenomenon occurs because the interface is curved, causing the water droplet to evaporate into the CO₂ phase (Hebach et al., 2002). The equilibrium vapor pressure for a curved interface that is concave towards the H₂O-rich phase is greater than that of a planar interface, so the water-saturated CO₂ phase is still undersaturated with respect to the small, high-curvature water droplet. There are two ways to circumvent this problem: the quasi-static

method (Hebach et al., 2002; Kvamme et al., 2007) and the equilibrium method (Bachu and Bennion, 2009; Chalbaud et al., 2009; Georgiadis et al., 2010). The quasi-static method uses an intermediate steady-state period during the time-evolution of IFT in which to make a measurement (Hebach et al., 2002; Kvamme et al., 2007). As its name implies, the equilibrium method entails pre-contacting the CO₂ and liquid water phases and further equilibrating individual drops to obtain an equilibrium interface shape (Bachu and Bennion, 2009). Reported equilibration times vary widely, from a few minutes (Chiquet et al., 2007a) to over 24 h (Bachu and Bennion, 2009).

1.5. High-quality data sets

In principle, all data sets conforming to the first two criteria mentioned above (directly-measured phase densities and appropriate thermocouple positioning) could be accepted regardless of the equilibration technique, but this latter factor likely introduces important uncertainty into the resulting IFT data. To the best of the authors' knowledge, only the measurements by Chiquet et al. (2007a) and Kvamme et al. (2007) meet all three criteria, so the availability of high-quality experimental IFT data encompassing the full range of relevant P and T conditions is in fact severely limited. Subsets of data from studies wherein $\Delta\rho$ is estimated and thermocouple positioning is correct (Massoudi and King, 1974; Hebach et al., 2002; Espinoza and Santamarina, 2010; Georgiadis et al., 2010) are acceptable at P – T conditions below 20 MPa and above 343 K. Of the high-quality data, only Georgiadis et al. (2010) and Chiquet et al. (2007a) performed experiments at high T , and only the Chiquet et al. (2007a) data refer to conditions directly comparable to the simulations presented in this study. As additional evidence of the quality of the Chiquet et al. (2007a) data set, there is excellent agreement between measurements of IFT as a function of pressure at 323 K reported independently by Chiquet et al. (2007a) and Kvamme et al. (2007), suggesting that their experimental data sets are consistent (Fig. 1). No direct comparison can be made between all accepted data sets, however, as there is no single temperature at which the IFT pressure dependence was investigated in all of these studies.

As noted parenthetically above, a fourth factor that could influence measured IFT data is the presence of impurities at the CO₂–water interface (Georgiadis et al., 2010). Impurity levels were not reported in published experimental CO₂–water IFT studies, but several results suggest that impurity levels were low in our critically selected database: our database is internally consistent (Fig. 1) and the results of Chiquet et al. (2007a) are consistent with those of Georgiadis et al. (2010), who took great care to suppress impurities in their experiments.

1.6. Simulations and models of IFT

Carbon dioxide–water phase relationships as well as the underlying molecular structure and dynamics have been explored using simulation techniques such as Monte Carlo (Destrienneville et al., 1996; Biscay et al., 2009) and

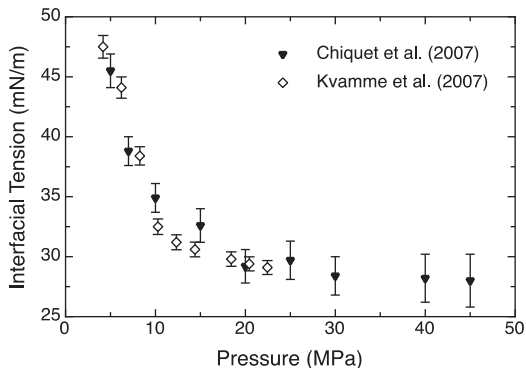


Fig. 1. Pressure dependence of IFT at 323 K determined experimentally by Chiquet et al. (2007a) and Kvamme et al. (2007). Uncertainty for the Chiquet et al. (2007a) measurements is reported in Chiquet et al. (2009).

molecular dynamics (In Het Panhuis et al., 1998; da Rocha and Johnston, 2001; Zhang and Duan, 2005; Duan and Zhang, 2006; Kvamme et al., 2007, 2009; Nieto-Draghi et al., 2007). Molecular simulations can be used to validate assumptions made in interpreting experimental data, to resolve discrepancies among published data sets, and to fill gaps where experimental data are lacking. Simulation results may also be used to distinguish the effects of molecular parameters on interfacial properties and thereby provide insight into the relationship between, say, IFT and the components of the CO₂-H₂O interaction. Molecular dynamics (MD) and Monte Carlo simulation techniques have long provided key insights of these kinds into the properties of water-air interfaces (Taylor et al., 1996; Tsuruta and Nagayama, 2004; Brown et al., 2008), but they have rarely been used to study water-CO₂ interfaces, perhaps because of the lack of well-tested CO₂-H₂O force fields. Moreover, to date it appears that no study has been performed comparing the quality of leading models of CO₂ and water in predicting IFT under the P - T conditions relevant to geologic CO₂ sequestration.

Interfacial tension between non-polar fluids and water has also been modeled using the gradient theory of fluid interfaces (Shah and Broseta, 2007; Lafitte et al., 2010), which provides a unified theory of fluid phase behavior and interfacial properties, given an equation of state and a set of fitted “influence parameters,” if the length scale of interfacial density gradients is much greater than intermolecular distances. The gradient theory modeling approach provides a good fit to experimental CO₂-water IFT data (Lafitte et al., 2010), but different insights into the molecular interactions controlling interfacial properties from what molecular simulations provide.

2. METHODS

2.1. Force field selection

Molecular dynamics simulations numerically solve the Newton-Euler equations of motion for a many-particle system and, therefore, they are well suited to investigating

dynamical, as well as structural and thermodynamic properties of many-particle systems. Intermolecular interactions are defined by force fields typically comprising short- and long-range components, accounting for van der Waals and Coulomb interactions respectively. The Lennard-Jones (LJ) 6-12 potential function is typically used to describe the short-range interactions:

$$U_{LJ} = 4\epsilon \left[\left(\frac{\sigma}{r} \right)^{12} - \left(\frac{\sigma}{r} \right)^6 \right] \quad (2)$$

where σ (Å) is the “hard-sphere” radius and ϵ (kJ/mol) defines the depth of the potential well. All model force fields tested in this paper treat atoms as charged LJ spheres assembled into rigid molecules.

Three leading CO₂ and two leading water force field models were compared as to the effect on IFT of varying LJ parameters and partial charges (Table 1). The DZ (Zhang and Duan, 2005; Duan and Zhang, 2006; Idrissi et al., 2007) and EPM2 (Harris and Yung, 1995; da Rocha and Johnston, 2001; Tegze et al., 2006; Kvamme et al., 2007; Nieto-Draghi et al., 2007) CO₂ model LJ parameters are nearly identical (Fig. 2), but the DZ model assigns considerably smaller partial charges to C and O atoms (Table 1). The PPL model (In Het Panhuis et al., 1998; Kvamme et al., 2009) short-range CO₂ interactions have larger ϵ and slightly larger σ than the others (Table 1) and the partial charges on CO₂ fall between those of the EPM2 and DZ models.

The SPC/E (Berendsen et al., 1987) and TIP4P2005 (Abascal and Vega, 2009) water models were also compared in our MD simulations. The SPC/E force field was chosen

Table 1

Partial charge and Lennard-Jones parameters (Eqs. (2)–(4)) for CO₂-CO₂ (DZ & EPM2) and H₂O-CO₂ interactions. The carbon dioxide C-O bond length is listed as l_{C-O} , and water oxygen is denoted by O_{SPC/E} and O_{TIP} for SPC/E (Berendsen et al., 1987) and TIP4P2005 (Abascal and Vega, 2005) water respectively. DZ-TIP4P2005 simulations were not performed in this study because of the similar behavior of the EPM2 and DZ models.

Parameter	EPM2 ^a		DZ ^b		PPL ^c	
q_C (e)	0.6512		0.5888		0.6172	
q_O (e)	-0.3256		-0.2944		-0.3086	
l_{C-O} (Å)	1.149		1.163		1.162	
Interaction	ϵ (kJ/mol)	σ (Å)	ϵ (kJ/mol)	σ (Å)	ϵ (kJ/mol)	σ (Å)
C-C	0.234	2.757	0.240	2.792	0.234	2.757
O-O	0.669	3.033	0.687	3.000	0.669	3.033
C-O	0.396	2.895	0.406	2.896	0.396	2.895
C-O _{SPC/E}	0.390	2.961	0.395	2.979	0.514	3.262
O-O _{SPC/E}	0.660	3.099	0.669	3.083	0.811	3.015
O _{SPC/E} ⁻	0.650	3.166	0.650	3.166	0.650	3.166
O _{SPC/E}						
C-O _{TIP}	0.426	2.958	–	–	0.514	3.262
O-O _{TIP}	0.720	3.096	–	–	0.811	3.015
O _{TIP} -O _{TIP}	0.775	3.159	–	–	0.650	3.159

^a Harris and Yung (1995).

^b Zhang and Duan (2005).

^c In Het Panhuis et al. (1998).

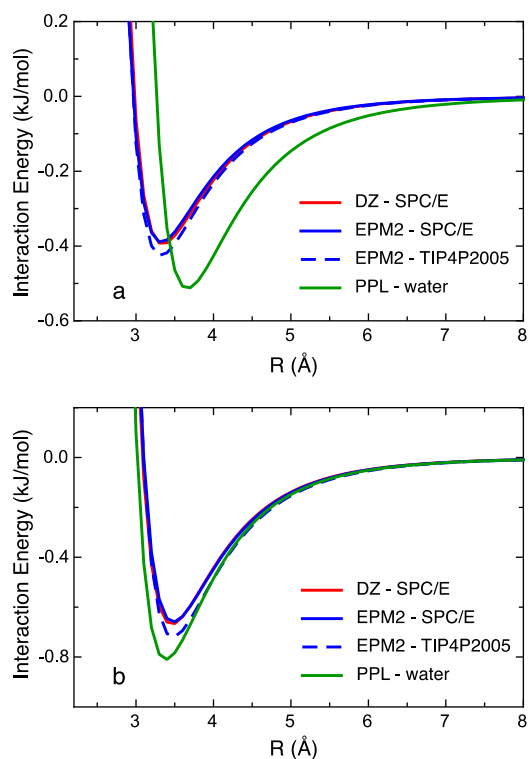


Fig. 2. Plot of the Lennard-Jones potential (Eq. (2)) as a function of distance for DZ-SPC/E, EPM2-SPC/E, EPM2-TIP4P2005, and PPL-water: C–O_w (a) and O_c–O_w (b). The label PPL-water represents the Lennard-Jones potential function for PPL-SPC/E and PPL-TIP4P2005, which are identical.

because of its ability to reproduce water self-diffusion, dissolved CO₂ solvent structure (In Het Panhuis et al., 1998), orthobaric density (Alejandre et al., 1995), static dielectric constant (Wasserman et al., 1995), and PVT properties up to high pressures (5–20 GPa; Duan and Zhang, 2006), and because it provides one of the best predictions of the liquid–vapor IFT of water (Chen and Smith, 2007; Vega and de Miguel, 2007). Despite some early now-controversial results indicating that the SPC/E model accurately reproduces the water surface tension (Alejandre et al., 1995), most simulations of water surface tension using the SPC/E force field underestimate surface tension by up to 10 mN/m (Chen and Smith, 2007; Vega and de Miguel, 2007). Indeed, most commonly used fixed-charge water models significantly underestimate the surface tension of liquid water. Only the TIP4P2005 water model has been shown to provide a better estimate of water surface tension (Vega and de Miguel, 2007), so this water model was also selected for comparison.

Because the surface tension of water directly affects the value of simulated interfacial tension, to obtain a quantitative prediction of IFT, it is necessary either to use the TIP4P2005 force field or to correct for the inaccuracy in the SPC/E water surface tension. Renormalization of simulation results using the SPC/E water model to have them correspond with the measured water surface tension presents an alternative to using the TIP4P2005 water model,

which is relatively new and has few reported interaction parameters with mineral atoms or aqueous solutes relevant to CO₂ storage in brine aquifers. Although the dependence of CO₂–water IFT on system pressure is controlled by the adsorption of CO₂ to the water surface (see discussion below), the zero-pressure value for this IFT must equal the surface tension of water at the temperature of interest. Thus increasing the SPC/E-simulated CO₂–water surface tension by $\Delta\gamma(T)$, the difference between the experimental and simulated surface tension of pure liquid water at a given temperature, may be used to renormalize IFT to reflect the values that would be obtained using a water model that reproduces the experimental water surface tension.

For the DZ and EPM2 model force fields, short-range CO₂–water interaction parameters (Fig. 2) were determined using the Lorentz–Berthelot combining rules:

$$\epsilon_{ij} = \sqrt{\epsilon_{ii}\epsilon_{jj}} \quad (3)$$

and

$$\sigma_{ij} = \frac{\sigma_{ii} + \sigma_{jj}}{2} \quad (4)$$

The Kong (1973) combining rules were also tested, but they did not improve agreement between our simulations and experiment. For the PPL model, EPM2 CO₂–CO₂ interactions were used, and short-range CO₂–H₂O interaction parameters were taken directly from In Het Panhuis et al. (1998) (Fig. 2). Thus, the strength of the PPL CO₂–H₂O interaction is the same for simulations using the SPC/E and TIP4P2005 water models.

2.2. Simulation methods

Simulations were performed with the code MOLDY 3.6 (Refson, 2004) using periodically-replicated cells containing 576 CO₂ molecules and 1152 H₂O molecules. Our simulation cells were 29 × 29 Å in directions parallel to the CO₂–water interface and at least 120 Å in the direction normal to the interface, which is sufficiently large to ensure that bulk phase properties are achieved in both fluid phases and that IFT is independent of system size (Taylor et al., 1996). A modified version of the Beeman algorithm (Beeman, 1976; Refson, 1985) is used to integrate the Newton–Euler equations with accuracy to $O(\delta t^4)$ in position and $O(\delta t^3)$ in velocity. Short-range forces are calculated within an intermolecular cutoff radius $r_c = 17.6$ Å. Long-range interactions are determined using three-dimensional Ewald summation (Refson, 2004).

Simulations were initialized by placing CO₂ and water phases, previously equilibrated as bulk phases for 0.5 ns at the appropriate P and T , into adjacent regions of the simulation cell. All MD simulations were then equilibrated in an NP_{*z*}E ensemble (i.e. fixed composition, interface-normal pressure, and energy) for 0.1 ns using a 0.1 fs timestep. During equilibration, rotational and translational velocities of all molecules were rescaled every 0.1 ps to reach the desired temperature, and the cell length (\bar{h}_z) along the CO₂–H₂O interface normal was allowed to vary according to the uniform-dilation limit of Parrinello–Rahman dynamics (Parrinello and Rahman, 1981; Refson, 2004). Simulations

were then run in an NVE ensemble (fixed composition, volume and energy) for 2 ns using a 0.001 ps timestep (e.g. Fig. 3). Drift in internal energy during each simulation was negligible ($<3 \times 10^{-5}$ kJ/mol).

The P - T conditions selected for our MD simulations encompassed the range of values relevant to geologic carbon storage, 310–383 K and 0–45 MPa (Chiquet et al., 2007a). For each model force field, the CO₂-H₂O system was simulated under the fixed pressure of 20 MPa at 300, 310, 323, 345, 373 and 383 K and under the fixed temperature of 383 K at 0 (CO₂-free), 3, 5, 10, 20, 30 MPa. The pressure chosen represents that above which experimental IFT values tend to reach a plateau (Chiquet et al., 2007a). Measured values of IFT are only weakly dependent on temperature above the CO₂ critical point (Kvamme et al., 2007; Chiquet et al., 2007a; Bachu and Bennion, 2009), so variable- P simulations were carried out at 383 K, the temperature at which the experimental IFT reaches its smallest value. We note in passing that the P - T conditions producing low IFT present the greatest risk of facilitating volume flow through cap rock.

2.3. Interfacial tension and surface excess

The value of IFT was calculated directly from the principal components of the MD simulation cell stress tensor using the relation:

$$\gamma = \frac{1}{2} \bar{h}_z \left[P_z - \frac{1}{2} (P_x + P_y) \right] \quad (5)$$

where P_z (Pa) is the interface-normal pressure, P_x and P_y (Pa) are interface-parallel pressures, and \bar{h}_z (m) is the interface-normal simulation cell length (Matsumoto and Kataoka, 1988; Kuznetsova and Kvamme, 2002). The simulation cell stress tensor is determined from the molecular virial by the MOLDY script. Our values of IFT reflect time-averaged principal stresses with uncertainty reported as two times the standard error of these values.

Molecular center-of-mass data were obtained from each simulation every 100 timesteps and imported into MATLAB for analysis. Simulation cells were divided into 500 slabs of equal length parallel to the z coordinate, and the number and type of molecular centers of mass within the slabs were counted at every timestep to determine the density profile (Fig. 3). Excess CO₂ adsorbed by the water surface was then quantified from the average of molecular center-of-mass output determined at each timestep using the equation:

$$\Gamma_{\text{CO}_2}^{(\text{H}_2\text{O})} = \frac{1}{A} \left[N_{\text{CO}_2} - \rho_{\text{CO}_2}^{\text{fl}} V^{\text{fl}} + \rho_{\text{CO}_2}^{\text{liq}} V^{\text{liq}} \right], \quad (6)$$

where A (m²) is the total interfacial area, N_{CO_2} is the number of CO₂ molecules, $\rho_{\text{CO}_2}^i$ (molecule/m³) is the number density of CO₂ in the bulk fluid region of phase i , V^i (m³) is volume of phase i and superscripts “fl” and “liq” stand for CO₂ and liquid water, respectively. Number density may be multiplied by (molecular weight)/(Avogadro’s number) to yield physical density (g/m³) for ease of interpretation. System size or N_{CO_2} does not affect the calculated surface excess as long as regions of bulk-fluid-like H₂O

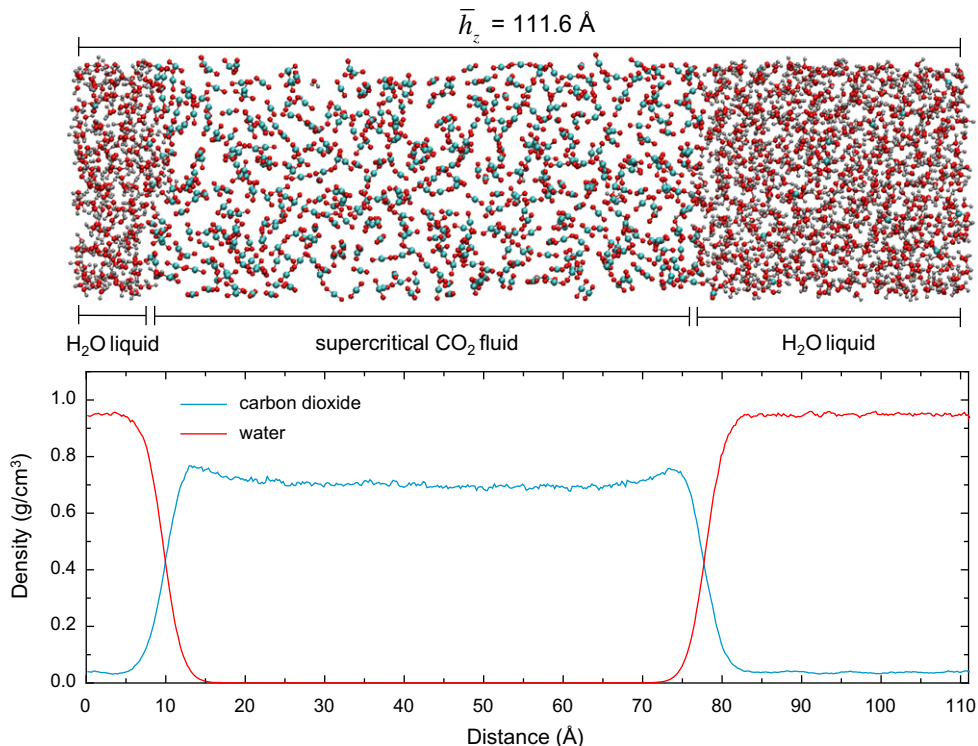


Fig. 3. (top) Molecular dynamics snapshot of an EPM2-SPC/E simulation equilibrated at 345 K and 20 MPa. Oxygen, carbon, and hydrogen atoms are represented by red, cyan, and gray spheres, respectively. The average cell length is 111.6 Å and the cell height and depth are both 28.9 Å. (bottom) Time-averaged density profile of the same simulation, with CO₂ fluid and liquid water bulk densities represented by flat profile regions. (For interpretation of the references to color in this figure legend, the reader is referred to the web version of this article.)

and CO₂ exist where ρ values are unaffected by the fluid–fluid interface. Bulk fluid phase densities were determined from regions where ρ values are invariant with z . In Fig. 3, this occurs at $z = 30$ to 60 and 90 to 100 Å for the CO₂ and H₂O phases, respectively. Interface positions and, therefore, phase volumes (V^{fl} and V^{liq}) were determined by defining the surface excess of water relative to water, $\Gamma_{\text{H}_2\text{O}}^{(\text{H}_2\text{O})}$, as 0 (IUPAC, 2001; Mucha et al., 2003). Given the definition of total cell volume,

$$V^{\text{fl}} + V^{\text{liq}} = A \cdot \bar{h}_z \quad (7)$$

it follows that

$$V^{\text{liq}} = \frac{N_{\text{H}_2\text{O}} - \rho_{\text{H}_2\text{O}}^{\text{fl}} V^{\text{fl}}}{\rho_{\text{H}_2\text{O}}^{\text{liq}}} = A \cdot \bar{h}_z - V^{\text{fl}} \quad (8)$$

Uncertainty propagated through these calculations increases with pressure because the region having the bulk CO₂ density becomes narrower relative to the water phase at higher pressures, due to the compressibility of the CO₂ fluid phase.

The IFT between two fluid phases is defined as the increase in the Gibbs energy per unit increase in interfacial surface area at constant P , T , and mole number (Butt et al., 2006). It exists as a consequence of the energetic penalty of decreasing the self-coordination of a molecule when it is removed from the bulk phase to an interface. Adsorption of molecules to a liquid–liquid or liquid–vapor interface directly affects IFT by reducing or enhancing this penalty. The relative surface excess of an adsorbed substance is directly related to IFT by the Gibbs adsorption equation. In a system with two components,

$$d\gamma = -\Gamma_2^{(1)} d\mu_2, \quad (9)$$

where $\Gamma_2^{(1)}$ (mol/m²) is the surface excess of a solute (2) relative to a solvent (1) and μ_2 (J/mol) is the solute chemical potential (c.f. Butt et al., 2006). Surface excess, a rapidly equilibrating property related directly to intermolecular forces, can be readily determined by MD simulation (Mucha et al., 2003). Comparison between simulated and measured CO₂ adsorption by a water surface thus may shed light on the quality of force field parameters.

Equation [9] may be applied to determine $\Gamma_{\text{CO}_2}^{(\text{H}_2\text{O})}$ using an experimental IFT vs. pressure curve. Accordingly, we calculated CO₂ surface excess from the Chiquet et al. (2007a) data by substituting the standard relation:

$$d\mu_{\text{CO}_2} = RT d \ln(f_{\text{CO}_2}) \quad (10)$$

into Eq. (9) to yield:

$$\Gamma_{\text{CO}_2}^{\text{H}_2\text{O}} = -\frac{f_{\text{CO}_2}}{RT} \frac{d\gamma}{df_{\text{CO}_2}} \quad (11)$$

where f_{CO_2} is the fugacity or unitless activity of CO₂ at a given external pressure and temperature, R is the ideal gas constant (J mol⁻¹ K⁻¹), and T is temperature (K). At high CO₂ pressure, non-ideality and therefore fugacity must be considered, while at sufficiently low pressure, fugacity must tend to equal P (Lewis and Randall, 1961). The fugacity at any temperature corresponding to a selected value of the pressure was calculated using an expression based on the

Redlich–Kwong equation of state for water–CO₂ mixtures published by Spycher et al. (2003). The slope of the experimental IFT vs. fugacity curve was calculated from the first derivative of an exponential fit to the data using the program proFit 6.1.3. Fitting parameters were sensitive to the 0 MPa surface tension of water, which was reported as 56.96 mN/m at 383 K (Vargaftik et al., 1983).

3. RESULTS AND DISCUSSION

3.1. Pressure and temperature dependence of IFT

All force field model combinations yield an IFT at 383 K that decreases notably with pressure as it is increased toward the CO₂ critical-point value of 7 MPa (Fig. 4a and b). Above the critical transition, IFT decreases more slowly with pressure, approaching a model-dependent constant value. The PPL-TIP4P2005 simulations of IFT are within the error of experimental values at all pressures (Fig. 4b). Renormalizing the PPL-SPC/E IFT values to the surface

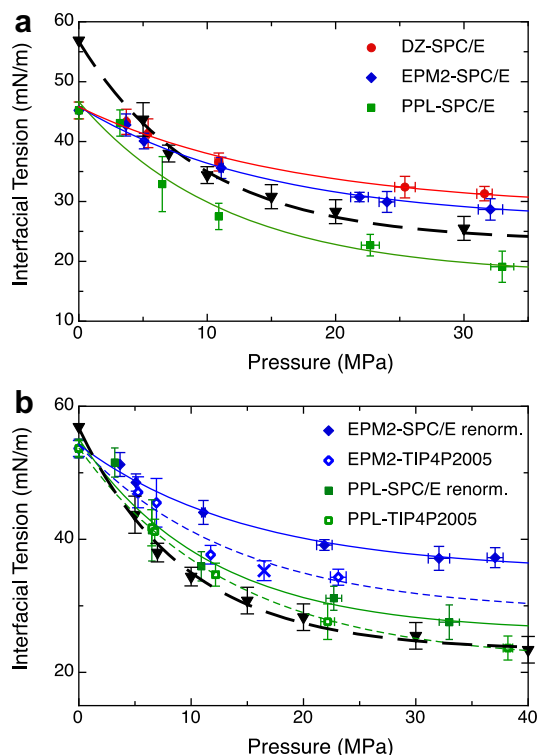


Fig. 4. Pressure dependence of IFT at 383 K calculated by MD simulation of (a) EPM2-, DZ- and PPL-SPC/E, and (b) EPM2- and PPL-TIP4P2005 compared with EPM2- and PPL-SPC/E IFT renormalized to TIP4P2005 water surface tension by adding the difference of experimental and simulated surface tension (8.4 mN/m at 383 K) to simulated IFT data. Curves through data represent exponential fits calculated using proFit. Corresponding experimental data are plotted as black triangles with a fitted black dashed curve. The blue X in (b) represents an EPM2-TIP4P2005 simulation at 383 K using the significantly larger simulation cell size and number of molecules used in Biscay et al. (2009). (For interpretation of the references to colour in this figure legend, the reader is referred to the web version of this article.)

tension of water generated by the TIP4P2005 model shifts simulated values upward by 8.4 mN/m to within the error of PPL-TIP4P2005 simulations (Fig. 4b). Both PPL curves then run approximately parallel to the experimental curve, indicating that the PPL CO₂-H₂O interaction best captures the pressure dependence of CO₂-water interfacial tension. The PPL CO₂-water interaction yields only slightly steeper slopes when the TIP4P2005 model is used instead of the SPC/E model.

Biscay et al. (2009) performed Monte Carlo (MC) simulations of EPM2-TIP4P2005 CO₂-H₂O interfacial tension and reported very good agreement of simulated IFT with experimental values at 383 K. Our results disagree with the Biscay et al. (2009) IFT results at 383 K and variable P , possibly due to employing different simulation methodologies, including simulation techniques, equilibration, simulation cell size and number of particles, and short-range interaction cutoff distance (12 Å in Biscay et al. (2009); 17.6 Å in this study). The asymmetric shape and absence of appreciable CO₂ in the water phase of density profiles presented by Biscay et al. (2009) suggest that their simulations may not have been fully equilibrated. To test the effect of simulation cell size on IFT, we performed an EPM2-TIP4P2005 simulation using the cell dimension and number of particles used by Biscay et al. (2009). This simulation yielded an IFT consistent with our IFT vs. P trend (blue X, Fig. 4b) and inconsistent with the reported Biscay et al. (2009) value. We performed a similar simulation using the cell dimension, number of molecules, and short-range cutoff distance used by Biscay et al. (2009), and found that decrease in cutoff distance had little effect. Thus we hypothesize that the degree of equilibration can significantly impact the simulated IFT.

The temperature dependence of IFT was evaluated at 20 MPa for all three CO₂ force fields with SPC/E water (Fig. 5). Experimentally, IFT at high pressures is only weakly dependent on temperature (Chiquet et al., 2007a; Chalbaud et al., 2009). Fig. 5 shows that IFT calculated with all three CO₂ models is also essentially temperature-independent. To account for the effect of the SPC/E model water surface tension on the temperature dependence of IFT, simulated and experimental IFT values may be renormalized to the measured water surface tension by adding the difference between experimental and simulated water surface tensions to simulated values at each temperature (Fig. 5b). The renormalized PPL-SPC/E IFT values again best approximate CO₂-water IFT measurements.

The similarity of IFT calculated with the EPM2 and DZ force fields (Figs. 4 and 5) is noteworthy because of the large differences between them in the partial charges they assign to CO₂ (Table 1). This finding suggests that the pressure dependence of IFT is insensitive to these partial charges and, therefore, to long-range Coulomb interactions. Accordingly, we can attribute the different behavior of the PPL force field to its relatively large ϵ_{C-Ow} and ϵ_{O-C-Ow} LJ parameters (Table 1), i.e., its short-range CO₂-H₂O interactions are strong, leading to a strong decrease in IFT with increasing pressure especially at low P . The similarity of PPL-TIP4P2005 and renormalized PPL-SPC/E IFT values supports this hypothesis, because both sets of simulations

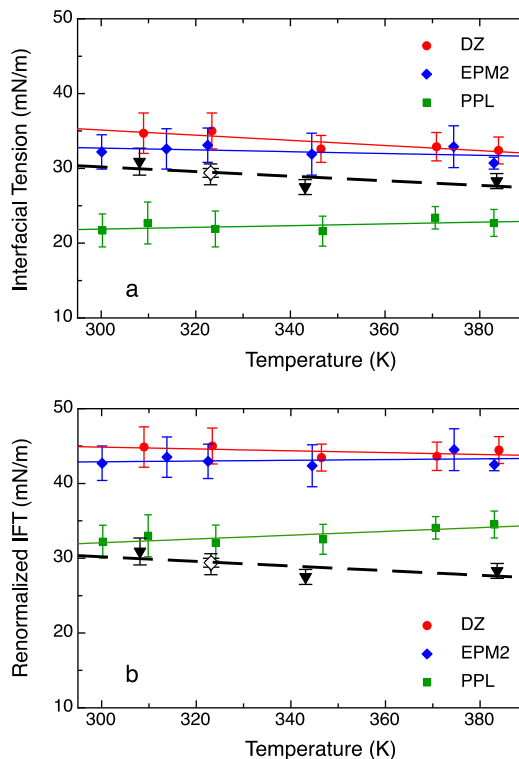


Fig. 5. Temperature dependence of IFT at 20 MPa calculated by MD simulation for (a) the DZ-, EPM2- and PPL-SPC/E force fields, and (b) the same data renormalized to experimental water surface tension by adding the difference of experimental and simulated surface tension at each temperature to simulated IFT data. Corresponding experimental data are plotted in black [Chiquet et al. (2007a), filled triangles; Kvamme et al. (2007), open diamond]. Simulated water surface tension values were determined for each simulation temperature based on a quadratic regression ($R^2 = 0.998$) of SPC/E surface tensions at 275, 300, 325, 350 K (Chen and Smith, 2007) and 383 K (this study).

use the same CO₂-H₂O interaction parameters and both predict a nearly identical IFT pressure dependence (Fig. 4b). Modification of short-range interactions appears to be the key to improving the CO₂-water interaction, as also shown by recent MC simulations of CO₂-water phase behavior (Vlcek et al., 2011).

3.2. The CO₂-water interface

Simulated CO₂-H₂O density profiles at the CO₂-H₂O interface show structure, with the density of CO₂ enhanced relative to its bulk value within 1 nm of the water surface (Figs. 3,6, with the SPC/E water model). As might be expected on the basis of the IFT comparisons, the strong short-range PPL CO₂-H₂O interaction results in the greatest CO₂ adsorption on the water surface, whereas the EPM2-SPC/E and DZ-SPC/E force fields yield similar CO₂ density profiles (Fig. 6).

Values of the relative surface excess of CO₂ calculated from simulation and those calculated from an exponential fit to the experimental fugacity dependence of IFT (Chiquet et al., 2007a; Eq. (11)) show a non-monotonic relationship

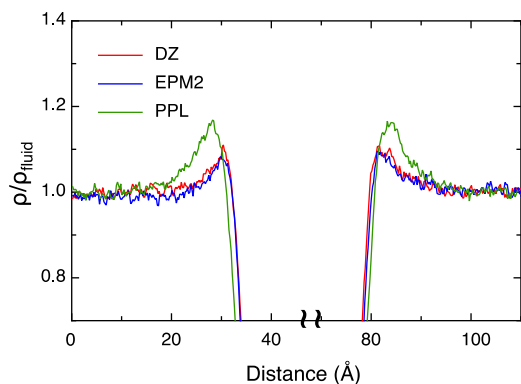


Fig. 6. Time-averaged supercritical CO₂ density at 345 K and 20 MPa normalized to the bulk fluid density as a function of distance along the simulation cell for simulations of DZ-, EPM2- and PPL-SPC/E. Near the interface, the CO₂ density is significantly enhanced (the water phase is located between 35 and 80 Å).

with pressure (Table 2 & Fig. 7). The increase of CO₂ surface excess with increasing pressure at low pressures and subsequent decrease of surface excess at high pressures can be understood quantitatively from Eq. (11), given the proportionality between fugacity and pressure and the increasing slope of IFT with increasing pressure (Fig. 4a). A non-monotonic relationship between CO₂ surface excess and pressure is consistent with previous measurements of the surface excess of CO₂ on solids (Cole et al., 2010).

The large CO₂ adsorption obtained for the PPL-SPC/E and PPL-TIP4P2005 simulations (relative to other force fields) translates to a surface excess greater than those calculated with the EPM2 and DZ force fields at all pressures (Fig. 7), a result evidently dependent mainly on short-range CO₂–H₂O interactions. In comparison with predicted experimental surface excess, the PPL model produces the best fit to the expected results for both water models. The slight increase in CO₂ surface excess observed in the PPL-TIP4P2005 simulations relative to PPL-SPC/E may result from the large increase and redistribution of charge on the water molecules in comparing the SPC/E model to the TIP4P2005 model. This increase is also consistent with the slight increase in slope of IFT vs. *P* observed when the TIP4P2005 water model is used instead of SPC/E (Fig. 4b).

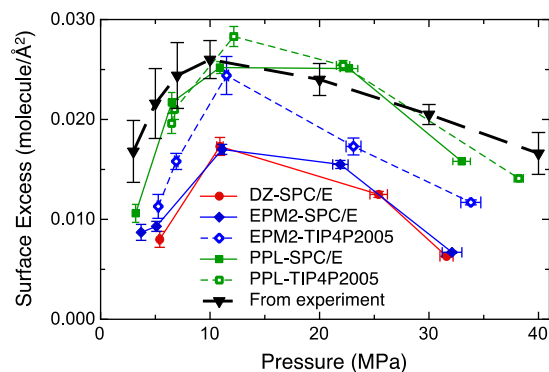


Fig. 7. Calculated CO₂ relative surface excess (molecule/Å²) as a function of pressure at 383 K according to the DZ-, EPM2-, and PPL-SPC/E models and the EPM2- and PPL-TIP4P2005 models. Surface excess predicted from the IFT data of Chiquet et al. (2007a) based on Eq. (11) using fugacity coefficients calculated from equations in Spycher et al. (2003) are plotted in black for comparison, with uncertainties based on the errors to exponential fitting coefficients calculated in proFit.

Despite the qualitative agreement between surface excess and the pressure dependence of IFT for all three models, the very good agreement between PPL-SPC/E surface excess and predicted experimental values is not expected, because the PPL-SPC/E simulations exhibit a slightly weaker pressure dependence of IFT than experiment (Fig. 4b). Surface excess does not exactly correspond to the slope of IFT vs. *P* at a given *P* and *T*, possibly due to the effect of capillary waves on the water surface causing variability (an increase) in interfacial area, which we did not take into account, or because of small differences between the fugacity coefficients of real vs. modeled CO₂.

The good agreement of the PPL-SPC/E and PPL-TIP4P2005 surface excess with values predicted from experiment (Fig. 7) may be explained qualitatively by examination of the interaction between CO₂ and randomly oriented water molecules. In the systems investigated here, carbon dioxide models located near the water surface have an almost random orientation relative to nearby water, because of the high temperature and the relatively weak CO₂–water interaction. Comparison with quantum mechanical predictions of the CO₂–H₂O dimer interaction potentials

Table 2

Relative surface excess of CO₂ ($\Gamma_{\text{CO}_2}^{(\text{H}_2\text{O})}$ in units of 10^{−3} molecule/Å²) at *T* = 383 ± 3 K as a function of pressure (MPa) determined from MD compared with values calculated from the slope of an exponential fit to experimental IFT data. Uncertainty is reported as 2 standard error (2SE). Simulation pressures are within ±15% of nominal *P*.

<i>P</i>	EPM2-SPC/E		DZ-SPC/E		PPL-SPC/E		EPM2-TIP4P2005		PPL-TIP4P2005		Predicted (<i>f</i>) ^a	
	Γ_{CO_2}	2SE	Γ_{CO_2}	2SE								
3	8.7	0.8	–	–	10.6	0.9	–	–	–	–	16.8	3.0
5	9.3	0.5	8.0	0.8	21.7	1.0	11.3	1.2	19.6	1.0	21.6	3.5
10	17.0	0.5	17.3	0.9	25.2	0.6	24.4	1.9	28.3	0.9	26.0	1.9
20	15.5	0.4	12.5	0.3	25.1	0.2	17.3	0.9	25.4	0.5	24.0	1.6
30	6.7	0.1	6.3	0.1	15.8	0.2	11.7	0.2	–	–	20.5	1.0

^a Surface excess CO₂ from the fugacity-dependence of experimental IFT (Chiquet et al., 2007a), with CO₂ fugacity calculated from the Spycher et al. (2003) equation of state.

(Sadlej et al., 1998; Duan and Zhang, 2006) averaged over all angular configurations reveal that the PPL model overestimates the short-range repulsive part of the CO₂-water interaction potential (i.e. it predicts larger molecules than implied by ab initio calculations). However, it correctly predicts the long-range attractive part of the CO₂-H₂O dimer interaction potential, which likely determines CO₂ adsorption on the water surface, whereas the EPM2 and DZ models underestimate the strength of this interaction.

In the range of temperatures and pressures relevant to CO₂ sequestration in brine aquifers and depleted hydrocarbon reservoirs, the PPL CO₂-water interaction most accurately captures calculated CO₂ surface excess and the measured pressure dependence of IFT. The PPL-SPC/E simulations adequately reproduce experimental IFT when renormalized to the surface tension of TIP4P2005 water, while PPL-TIP4P2005 simulations reproduce both experimental water surface and interfacial tension extremely well without renormalization. However, because of the greater abundance of well-tested solute- and mineral-water interaction potentials available for use with SPC/E water, the PPL-SPC/E model may have greater utility than the PPL-TIP4P2005 model for studying CO₂-brine-mineral systems relevant to geologic CO₂ storage.

ACKNOWLEDGMENTS

This material is based upon work supported as part of the Center for Nanoscale Control of Geologic CO₂, an Energy Frontier Research Center funded by the U.S. Department of Energy, Office of Science, Office of Basic Energy Sciences under Award No. DE-AC02-05CH11231.

REFERENCES

- Abscal J. L. F. and Vega C. (2005) General purpose model for the condensed phases of water: TIP4P/2005. *J. Chem. Phys.* **123**, 1–12, 234505.
- Aggelopoulos C. A., Robin M., Perfetti E. and Vizika O. (2010) CO₂/CaCl₂ solution interfacial tensions under geologic CO₂ storage conditions: influence of cation valence on interfacial tension. *Adv. Water Res.* **33**, 691–697.
- Alejandre J., Tildesley D. J. and Chapela G. A. (1995) Molecular dynamics simulation of the orthobaric densities and surface tension of water. *J. Chem. Phys.* **102**, 4574–4583.
- Alkan H., Cinar Y. and Ülker E. B. (2010) Impact of capillary pressure, salinity and in situ conditions on CO₂ injection into saline aquifers. *Transp. Porous Media* **84**, 799–819.
- André L., Audigane P., Azaroual M. and Menjot A. (2007) Numerical modeling of fluid-rock chemical interactions at the supercritical CO₂-liquid interface during CO₂ injection into a carbonate reservoir, the Dogger aquifer (Paris Basin, France). *Energy Convers. Manage.* **48**, 1782–1797.
- Andreas J. M., Hauser E. A. and Tucker W. B. (1938) Boundary tension by pendant drops. *J. Phys. Chem.* **42**, 1001–1019.
- Bachu S. (2000) Sequestration of CO₂ in geological media: criteria and approach for site selection in response to climate change. *Energy Convers. Manage.* **41**, 953–970.
- Bachu S. and Bennion D. B. (2009) Interfacial tension between CO₂, freshwater and brine in the range of pressure from (2 to 27) MPa, temperature from (20 to 125) °C, and water salinity from (0 to 334,000) mg L⁻¹. *J. Chem. Eng. Data* **54**, 765–775.
- Beeman D. (1976) Some multistep methods for use in molecular dynamics calculations. *J. Comput. Phys.* **20**, 130–139.
- Berendsen H., Grigera J. and Straatsma T. (1987) The missing term in effective pair potentials. *J. Phys. Chem.* **91**, 6269–6271.
- Biscay F., Ghoufi A., Lachet V. and Malfreyt P. (2009) Monte Carlo simulations of the pressure dependence of the water-acid gas interfacial tensions. *J. Phys. Chem. B* **113**, 14277–14290.
- Brown M. A., D'Auria R., Kuo I.-F. W., Krisch M. J., Starr D. E., Bluhm H., Tobias D. J. and Hemminger J. C. (2008) Ion spatial distributions at the liquid-vapor interface of aqueous potassium fluoride solutions. *Phys. Chem. Chem. Phys.* **10**, 4778–4784.
- Butt H., Graf K. and Kappl M. (2006) *Physics and Chemistry of Interfaces*. Wiley-VCH, Weinheim.
- Chalbaud C., Robin M., Lombard J.-M., Martin F., Egermann P. and Bertin H. (2009) Interfacial tension measurements and wettability evaluation for geological CO₂ storage. *Adv. Water Res.* **32**, 98–109.
- Chen F. and Smith P. E. (2007) Simulated surface tensions of common water models. *J. Chem. Phys.* **126**, 1–3, 221101.
- Chiquet P., Daridon J.-L., Broseta D. and Thibeau S. (2007a) CO₂/water interfacial tensions under pressure and temperature conditions of CO₂ geological storage. *Energy Convers. Manage.* **48**, 736–744.
- Chiquet P., Broseta D. and Thibeau S. (2007b) Wettability alteration of caprock minerals by carbon dioxide. *Geofluids* **7**, 112–122.
- Chiquet P., Daridon J.-L., Broseta D. and Thibeau S. (2009) Erratum to the paper “CO₂/water interfacial tensions under pressure and temperature conditions of CO₂ geological storage”. *Energy Convers. Manage.* **50**(2), 431.
- Chun B.-S. and Wilkinson G. T. (1995) Interfacial tension in high-pressure carbon dioxide mixtures. *Ind. Eng. Chem. Res.* **34**, 4371–4377.
- Cole D. R., Chialvo A. A., Rother G., Vlcek L. and Cummings P. T. (2010) Supercritical fluid behavior at nanoscale interfaces: implications for CO₂ sequestration in geologic formations. *Philos. Mag.* **90**(17–18), 2339–2363.
- Da Rocha S. R. P. and Johnston K. P. (2001) Molecular structure of the water-supercritical CO₂ interface. *J. Phys. Chem. B* **105**, 12092–12104.
- Da Rocha S. R. P., Harrison K. L. and Johnston K. P. (1999) Effects of surfactants on the interfacial tension and emulsion formation between water and carbon dioxide. *Langmuir* **15**, 419–428.
- Destigneville C. M., Brodhold J. P. and Wood B. J. (1996) Monte Carlo simulation of H₂O-CO₂ mixtures to 1073.15 K and 30 kbar. *Chem. Geol.* **133**, 53–65.
- Duan Z. and Zhang Z. (2006) Equation of state of the H₂O, CO₂ and H₂O-CO₂ systems up to 10 GPa and 2573.15 K: molecular dynamics simulations with ab initio potential surface. *Geochim. Cosmochim. Acta* **70**, 2311–2324.
- Espinosa D. N. and Santamarina J. C. (2010) Water-CO₂-mineral systems: interfacial tension, contact angle, and diffusion – Implications to CO₂ geological storage. *Water Resour. Res.* **46**, W07537. doi:10.1029/2009WR008634.
- Georgiadis A., Maitland G., Trusler J. P. M. and Bismarck A. (2010) Interfacial tension measurements of the (H₂O + CO₂) system at elevated pressures and temperatures. *J. Chem. Eng. Data* **55**, 4168–4175.
- Hauser E. A. and Michaels A. S. (1948) Interfacial tension at elevated pressures and temperatures. I. A. New apparatus for boundary-tension measurements by the pendent drop method. *J. Phys. Chem.* **52**, 1157–1165.

- Harris J. G. and Yung K. H. (1995) Carbon dioxide's liquid–vapor coexistence curve and critical properties as predicted by a simple molecular model. *J. Phys. Chem.* **99**, 12021–12024.
- Hebach A., Oberhof A., Dahmen N., Kögel A., Ederer H. and Dinjus E. (2002) Interfacial tension at elevated pressures – measurements and correlations in the water + carbon dioxide system. *J. Chem. Eng. Data* **47**, 1540–1546.
- Heuer G. (1957) Interfacial tension of water against hydrocarbon and other gases and adsorption of methane on solids at reservoir temperatures and pressures. Ph. D. thesis, Univ. Texas Austin.
- Idrissi A., Damay P. and Kiselev M. (2007) Nearest neighbor assessments of spatial distribution in CO₂: a molecular dynamics analysis. *Chem. Phys.* **332**, 139–143.
- In Het Panhuis M., Patterson C. H. and Lynden-Bell R. M. (1998) A molecular dynamics study of carbon dioxide in water: diffusion, structure and thermodynamics. *Mol. Phys.* **94**, 963–972.
- IPCC (2005) *IPCC special report on carbon dioxide capture and storage* (eds. B. Metz, O. Davidson, H. de Coninck, M. Loos, and L. Meyer) Cambridge Univ. Press, New York.
- IUPAC (2001) *Adsorption at the fluid/fluid interface*.
- Kong C. L. (1973) Combining rules for intermolecular potential parameters. II. Rules for Lennard-Jones (12–6) potential and the Morse potential. *J. Chem. Phys.* **59**, 2464–2467.
- Kuznetsova T. and Kvamme B. (2002) Thermodynamic properties and interfacial tension of a model water–carbon dioxide system. *Phys. Chem. Chem. Phys.* **4**, 937–941.
- Kvamme B., Kuznetsova T., Hebach A., Oberhof A. and Lunde E. (2007) Measurements and modeling of interfacial tension for water + carbon dioxide systems at elevated pressures. *Comput. Mater. Sci.* **38**, 506–513.
- Kvamme B., Kuznetsova T. and Uppstad D. (2009) Modeling excess surface energy in dry and wetted calcite systems. *J. Math. Chem.* **46**, 756–762.
- Lafitte T., Mendiboure B., Piñeiro M. M., Bessières D. and Miquieu C. (2010) Interfacial properties of water/CO₂: a comprehensive description through a gradient theory – SAFT-VR Mie approach. *J. Phys. Chem. B* **114**, 11110–11116.
- Leroy P., Lassin A., Azaroual M. and André L. (2010) Predicting the surface tension of aqueous 1:1 electrolyte solutions at high salinity. *Geochim. Cosmochim. Acta* **74**, 5427–5442.
- Lewis G. N. and Randall M. (1961) *Thermodynamics*, 2nd ed. Rev. McGraw-Hill, New York.
- Li S., Dong M., Li Z., Huang S., Qing H. and Nickel E. (2005) Gas breakthrough pressure for hydrocarbon reservoir rocks: Implications for the security of long-term CO₂ storage in the Weyburn field. *Geofluids* **5**, 326–334.
- Li Z., Dong M., Li S. and Huang S. (2006) CO₂ sequestration in depleted oil and gas reservoirs – caprock characterization and storage capacity. *Energy Convers. Manage.* **47**, 1372–1382.
- Li X.-S., Liu J.-M. and Fu D. (2008) Investigation of interfacial tensions for carbon dioxide aqueous solutions by perturbed-chain statistical associating fluid theory combined with density-gradient theory. *Ind. Eng. Chem. Res.* **47**, 8911–8917.
- Massoudi R. and King, Jr., A. D. (1974) Effect of pressure on the surface tension of water. Adsorption of low molecular weight gases on water at 25°. *J. Phys. Chem.* **78**(22), 2262–2266.
- Matsumoto M. and Kataoka Y. (1988) Study on liquid–vapor interface of water. I. Simulational results of thermodynamic properties and orientational structure. *J. Chem. Phys.* **88**(5), 3233–3245.
- Mucha M., Hrobárik T. and Jungwirth P. (2003) Surface tension from molecular dynamics simulation: adsorption at the gas–liquid interface. *Isr. J. Chem.* **43**, 393–397.
- Nieto-Draghi C., de Bruin T., Pérez-Pellitero J., Avalos J. B. and Mackie A. D. (2007) Thermodynamic and transport properties of carbon dioxide for molecular simulation. *J. Chem. Phys.* **126**, 064509.
- Parrinello M. and Rahman A. (1981) Polymorphic transitions in single crystals: a new molecular dynamics method. *J. App. Phys.* **52**(12), 7182–7190.
- Pentland C. H., El-Maghraby R., Iglauer S. and Blunt M. J. (2011) Measurements of the capillary trapping of super-critical carbon dioxide in Berea sandstone. *Geophys. Res. Lett.* **38**, 1–4.
- Refson, K. (2004) *Moldy user's manual*.
- Refson K. (1985) Molecular dynamics simulation of solid *n*-butane. *Physica* **131B**, 256–266.
- Sadlej J., Makarewicz J. and Chałasiński G. (1998) *Ab initio* study of energy, structure, and dynamics of the water–carbon dioxide complex. *J. Chem. Phys.* **109**(10), 3919–3927.
- Shah V. and Broseta D. (2007) Predicting interfacial tension between water and nonpolar fluids from a Cahn-type theory. *Langmuir* **23**, 12598–12605.
- Siemons N., Bruining H., Castelijn H. and Wolf K.-H. (2006) Pressure dependence of the contact angle in a CO₂–H₂O–coal system. *J. Colloid Interface Sci.* **297**, 755–761.
- Spycher N., Pruess K. and Ennis-King J. (2003) CO₂–H₂O mixtures in the geological sequestration of CO₂. I. Assessment and calculation of mutual solubilities from 12 to 100° C and up to 600 bar. *Geochim. Cosmochim. Acta* **67**(16), 3015–3031.
- Suekane T., Zhou N., Hosokawa T. and Matsumoto T. (2010) Direct observation of trapped gas bubbles by capillarity in sandy porous media. *Transp. Porous Med.* **82**, 111–122.
- Taylor R. S., Dang L. X. and Garrett B. C. (1996) Molecular dynamics simulations of the liquid/vapor interface of SPC/E water. *J. Phys. Chem.* **100**, 11720–11725.
- Tewes F. and Boury F. (2004) Thermodynamic and dynamic interfacial properties of binary carbon dioxide – water systems. *J. Phys. Chem. B* **108**, 2405–2412.
- Tegze G., Pusztai T., Tóth G., Gránágy L., Svandal A., Buanes T., Kuznetsova T. and Kvamme B. (2006) Multiscale approach to CO₂ hydrate formation in aqueous solution: phase field theory and molecular dynamics. Nucleation and growth. *J. Chem. Phys.* **124**, 234710.
- Tsuruta T. and Nagayama G. (2004) Molecular dynamics studies on the condensation coefficient of water. *J. Phys. Chem. B* **108**, 1736–1743.
- Vargaftik N. B., Volkov B. N. and Voljak L. D. (1983) International tables of the surface tension of water. *J. Phys. Chem. Ref. Data* **12**(3), 817–820.
- Vega C. and de Miguel E. (2007) Surface tension of the most popular models of water by using the test-area simulation method. *J. Chem. Phys.* **126**, 154707.
- Vlcek L., Chialvo A. A. and Cole D. R. (2011) Optimized unlike-pair interactions for water–carbon dioxide mixtures described by the SPC/E and EPM2 models. *J. Phys. Chem. B* **115**, 8775–8784.
- Wasserman E., Wood B. and Brodholt J. (1995) The static dielectric constant of water at pressures up to 20 kbar and temperatures to 1273 K: experiment, simulations, and empirical equations. *Geochim. Cosmochim. Acta* **59**(1), 1–6.
- Wesch A., Dahmen N., Ebert K. and Schön J. (1997) Grenzflächenspannungen, tropfengrößen und kontaktwinkel im zwei-phasesystem H₂O/CO₂ bei temperaturen von 298 bis 333 K und drücken bis 30 MPa. *Chem. Ing. Tech.* **69**, 942–946.
- Zhang Z. and Duan Z. (2005) An optimized molecular potential for carbon dioxide. *J. Chem. Phys.* **122**, 214507.